Frontiers of Physics
https://doi.org/10.1007/s11467-019-0924-1
Front. Phys.
14(5), 52603 (2019)

RESEARCH ARTICLE

Controllable electromagnetically induced grating in a cascade-type atomic system

Jin-Peng Yuan[1,2], Chao-Hua Wu[1,2], Yi-Hong Li[1,2], Li-Rong Wang[1,2,†], Yun Zhang[3,‡], Lian-Tuan Xiao[1,2], Suo-Tang Jia[1,2]

[1] *State Key Laboratory of Quantum Optics and Quantum Optics Devices, Institute of Laser Spectroscopy, Shanxi University, Taiyuan 030006, China*
[2] *Collaborative Innovation Center of Extreme Optics, Shanxi University, Taiyuan 030006, China*
[3] *Department of Engineering Science, The University of Electro-Communications, 1-5-1 Chofugaoka, Chofu-shi, Tokyo, 182-8585, Japan*
Corresponding authors. E-mail: [†] *wlr@sxu.edu.cn,* [‡] *zhang@ee.uec.ac.jp*
Received July 30, 2019; accepted August 19, 2019

A controllable electromagnetically induced grating (EIG) is experimentally realized in a coherent rubidium ensemble with $5S_{1/2}$–$5P_{3/2}$–$5D_{5/2}$ cascade configuration. In our work, a whole picture describing the relation between the first-order diffraction efficiency and the power of the coupling field is experimentally presented for the first time, which agrees well with the theoretical prediction. More important, by fine tuning the experimental parameters, the first-order diffraction efficiency of as high as 25% can be achieved and a clear three-order diffraction pattern is also observed. Such a controllable periodic structure can provide a powerful tool for studying the control of light dynamics, pave the way for realizing new optical device.

Keywords coherent optical effects, diffraction gratings, multiphoton processes

1 Introduction

Atomic coherence and quantum interference play an important role in quantum optics and laser physics. With the ability of controlling the response of the medium to the optical field by a strong laser field, many fascinating phenomena were extensively investigated in the past two decades owing to enormous promising applications [1]. Under limited conditions, the absorption of the probe laser vanishes, which is known as electromagnetically induced transparency (EIT) [2]. In the EIT related systems, important applications have been studied in quantum devices and quantum information [3–6].

When the traveling wave field of EIT is replaced by a standing-wave field, the atomic coherence of medium is modulated periodically in the space and the weak probe field can be diffracted into high order patterns. This phenomenon is named as electromagnetically induced grating (EIG) [7]. Compared with the traditional grating, the EIG configuration can be easily constructed and flexibly tuned, thus the properties of light propagation can be directly controlled. Furthermore, the observation of EIG spectra is background free with no associated dark current [8]. EIG has various applications in realizing all-optical communication, such as all optical switching, routing and light storage [9–11], probing material optical properties [12], photonic bandgaps [13], atomic/molecular velocimetry [14], realizing optical bistability [15], beam splitting and fanning [16], shaping a biphoton spectrum [17].

As a matter of fact, the EIG was experimentally realized in a three-level Λ system of cold sodium atoms [18] and an optical-pumping-transferred ground-state population grating was conducted in cold cesium atoms [14]. A discrete diffraction of the light propagation and an all-optical two-port signal router-all-optical switch based on EIG were also demonstrated in a vapor cell [9, 19, 20]. Moreover, a four-level ladder-type atomic system, an asymmetric semiconductor quantum well structure, a three-level ladder-type hybrid artificial molecule and other systems are also theoretically suggested for the realization of EIG [21–27]. However, the previous experiments are all focusing on the phenomenon realization, the research on the grating controllability, especially the diffraction efficiency, receives less attention. A high diffraction efficiency is required for developing all-photonic devices based on EIG. A microwave-driven four-level atomic system, a four-level N-type atomic system, a four-level double V-type quantum system and a graphene ensemble are theoretically proposed for the realization of a high efficiency EIG [28–31]. Because the EIG is a hybrid grating with synchronous modulations on amplitude and phase, the EIT related parameters, such as two-photon detuning and coupling laser power, should be taken into account to improve the diffraction efficiency of the grating.

In this paper, we studied EIG in a coherent $5S_{1/2}$–

$5P_{3/2}$–$5D_{5/2}$ ^{85}Rb atomic ensemble. A weak probe laser propagates perpendicular to the standing-wave coupling field, which is formed by two coupling lasers symmetrically intersected with a small angle in the vapor. Thus, the distinct diffraction patterns are observed with high resolution. The grating controllability are systematically studied with experimental parameters such as, angle of the two coupling lasers, two-photon detuning and coupling laser power. A high first-order diffraction efficiency of 25 % is obtained and the distinguished three-order diffraction is observed. Owning to the high diffraction efficiency and multi-parameter controllability, this atomic ensemble provides potential applications in all-optically manipulating the propagation of light field and developing all-photonic devices.

2 Experiment setup

The related ^{85}Rb energy levels diagram is shown in Fig. 1(b). A weak probe field with Rabi frequency Ω_p and detuning $\Delta_p = \omega_p - \omega_{21}$ drives the $5S_{1/2}$–$5P_{3/2}$ transition. A strong coupling field with Rabi frequency Ω_c and detuning $\Delta_c = \omega_c - \omega_{32}$ couples the $5P_{3/2}$–$5D_{5/2}$ transition. The atoms in $5D_{5/2}$ states decay back to $5S_{1/2}$ state via $6P_{3/2}$ intermediate state and a 420 nm fluorescence simultaneously emits from the spontaneous radiation of $6P$–$5S$ transition.

The experiment setup is shown in Fig. 1(a). A diode laser (DL pro, Toptica) operating at 776 nm, corresponding to coupling field, is split by a polarization beam splitter (PBS1) into two beams. One beam enters into a commercial Fabry-Perot interferometer for frequency stabilization, and the output frequency is monitored by a wavelength meter (WS-7, HighFinesse). The other beam is further split into two beams by PBS2. The beam with low power is used to obtain the EIT signal, and the other beam is shaped into an elliptical profile by an anamorphic prism pair (AP). The shaped beam is split into two beams by a beam-splitter (BS1) resulted in same profile and power, and then the two beams are symmetrically recombined together with a small angle 2φ in the center of a rubidium

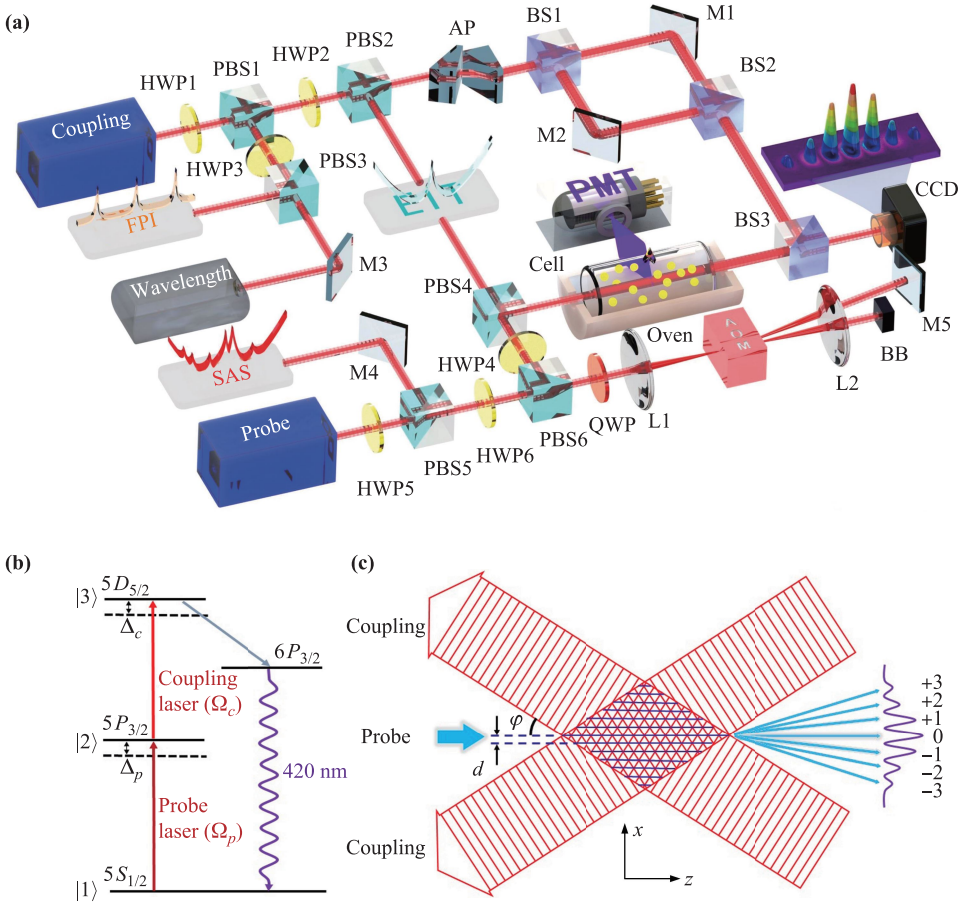

Fig. 1 **(a)** Experiment setup, HWP: Half-wave plate, PBS: Polarization beam splitter, AP: Anamorphic prism, BS: Beam splitter, M: High reflection mirror, FPI: Fabry–Perot interferometer, EIT: Electromagnetically induced transparency, PMT: photomultiplier tube, SAS: Saturation absorption spectroscopy, CCD: Charge-coupled device, QWP: Quarter-wave plate, L: Lens, AOM: Acousto–optic modulator, BB: Beam block. **(b)** Schematic diagram of a cascade-type coherent rubidium system. **(c)** Illustration of electromagnetically induced grating by a standing-wave (x direction) coupling field and a traveling wave (z direction) probe field.

vapor cell. Then a standing-wave field appears in the x direction perpendicular to the propagation direction of the probe field, which is illustrated in Fig. 1(c). The grating constant is $d = \lambda_c/(2\sin\varphi)$, where λ_c is the wavelength of the coupling laser. The pure ^{85}Rb vapor cell is 2.5 cm in diameter and 10 cm in length, and it can be heated by an oven, the temperature of the oven is precisely controlled within 0.1 K. The frequency of diode laser (DL pro, Toptica) operating at Rb D2 line (780nm), serving as probe field, is locked by saturation absorption spectroscopy. The frequency locked beam passes through a double-pass configuration based on an acousto-optical modulator (AOM), during which its frequency is detuned and its polarization is rotated by a quarter-wave plate. The frequency detuned beam is then split by PBS4, the transmitted beam is used to obtain the EIT signal together with the coupling laser. The reflected beam propagates through the vapor cell along the z direction. With the standing-wave field formed in x direction, the probe beam will be diffracted into high order patterns. The diffraction pattern of the probe laser is observed by a commercial charge-coupled device (CCD). A photomultiplier tube is placed near the vapor cell to collect the 420 nm fluorescence [32], which is used to monitor the coherence of atomic system.

3 Results and discussion

The susceptibility of this system can be expressed as [7]

$$\chi = \frac{\mathrm{i}N|\mu_{12}|^2}{\hbar\varepsilon_0}\left[\frac{\Gamma_{31}}{2} - \mathrm{i}\Delta_p + \frac{|\Omega_c|^2\cos(\pi x/d)}{\Gamma_{32}/2 - \mathrm{i}(\Delta_p+\Delta_c)}\right]^{-1}, \tag{1}$$

where N is the atomic ensemble density and Γ_{ij} is the decay rate between states $|i\rangle$ and $|j\rangle$, here Γ_{31} and Γ_{32} are $2\pi\times 0.66$ MHz and $2\pi\times 6.066$ MHz, respectively. $\mu_{12} = 4.22753(87)\ \mathrm{ea_0}$ is the transition dipole momentum between the levels $|1\rangle$ and $|2\rangle$. Under the slowly varying approximation and the steady-state regime, the propagation of the probe field along the z direction using Maxwell's equation can be written as

$$\frac{\partial E_p}{\partial z} = (\alpha + \mathrm{i}\beta)E_p, \tag{2}$$

where $\alpha = (-2\pi/\lambda)\chi''$ and $\beta = (2\pi/\lambda)\chi'$ are the absorption and dispersion coefficients of the probe field, respectively. Here we consider $\chi = \chi' + \mathrm{i}\chi''$. For simplification and focus on characteristics of EIG, the transverse part of Eq. (2) has been ignored. By solving Eq. (2), the transmission function of the modulated probe field at $z = L$ can easily be calculated analytically and is given by

$$E_p(x,L) = E_p(x,0)T_{amp}(x)T_{phase}(x), \tag{3}$$

where $T_{amp}(x) = \mathrm{e}^{\alpha(x)L} = \mathrm{e}^{-2\pi L\chi''/\lambda_p}$ and $T_{phase}(x) = \mathrm{e}^{\mathrm{i}\beta(x)L} = \mathrm{e}^{\mathrm{i}2\pi L\chi'/\lambda_p}$ denote the amplitude and phase modulation respectively and $E_p(x,0)$ is the input probe profile. The Fourier transformation of $E_p(x,L)$ then yields the Fraunhofer or far-field intensity diffraction equation

$$I_p(\theta) = |E_p(\theta)|^2 \times \frac{\sin^2(M\pi R\sin\theta)}{M^2\sin^2(\pi R\sin\theta)}, \tag{4}$$

with $E_p(\theta) = \int_{-d/2}^{d/2} E_p(x,L)\mathrm{e}^{-\mathrm{i}2\pi xR\sin\theta}\mathrm{d}x$ denotes the Fraunhofer diffraction of a single period and $R = d/\lambda_p$. In addition, θ denotes the diffraction angle of probe beam with respect to the z direction while M represents the ratio between the beam width and the grating period. The nth-order diffracted probe field can be found at an angle determined by $n = R\sin\theta \in (\cdots, -1, 0, 1, \cdots)$. Considering the first-order diffraction ($n = 1$) case, the intensity diffraction equation is

$$I_p^1(\theta) = |E_p^1(\theta)|^2 = \left|\int_{-\frac{d}{2}}^{\frac{d}{2}} E_p(x,L)\mathrm{e}^{-\mathrm{i}2\pi x}\mathrm{d}x\right|^2. \tag{5}$$

Specifically, we can calculate the first-order diffraction intensity according to Eq. (5). Note that it is associated with the input probe profile $E_p(x,0)$. In the theoretical simulation, we assume the input probe field is a plane wave for simplicity and the value of Eq. (5) amounts to the first-order diffraction efficiency.

The experimental demonstration of the EIG phenomenon is performed by investigating the output profile of the incident probe beam. Figure 2(a) is the experimentally measured intensity distribution of probe beam in absence of the standing-wave coupling field. The spatial intensity distribution shows in the main picture is actually the section profile of the output pattern versus x axis. The inset is the direct output profile from the CCD, and the dotted line notifies the position of the section. The related experimental parameters are as follows, the probe field power is 1.7 mW and its frequency is blue detuned 20 MHz to $5S_{1/2}(F=2) - 5P_{3/2}(F=2)$ hyperfine transition, the temperature of vapor cell is 377.6 K. When the standing-wave coupling field is established by the interference of two coupling lasers with small angle of $2\varphi \approx 0.4$ degree, an EIG is clearly emerged, which can

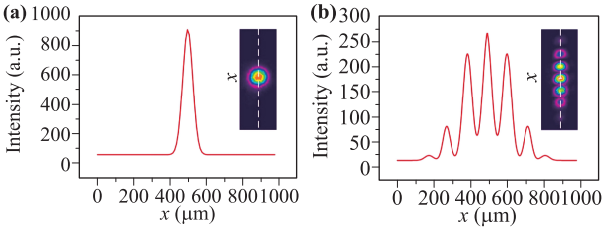

Fig. 2 The spatial intensity distribution of probe beam through the vapor cell without **(a)**/with **(b)** the standing-wave field. The line is the intensity distribution of the section profile of the output pattern versus x axis. The inset is the direct output profile of the probe beam from the CCD, and the dotted line notifies the position of the section.

be clearly observed in the inset of Fig. 2(b). The coupling laser power is 16 mW and its frequency resonances with $5P_{3/2}(F = 2) - 5D_{5/2}(F = 1)$ hyperfine transition. Figure 2(b) gives out the spatial intensity distribution of the probe laser after being diffracted by the grating. The distinguished third-order diffraction pattern is observed and the high diffraction efficiency of the grating is achieved.

We can simultaneously get the intensity and spatial distributions of each order from Fig. 2(b). The intensity distribution presents the diffraction efficiency while the spatial distribution gives the grating constant. With the coupling laser wavelength of 776 nm, and the crossed angle of $2\varphi \approx 0.4$ degree, the grating constant is calculated as 111 μm. The grating constant is characterized by the spacing between two adjacent diffraction patterns in the experimental result. With the measured spacing and the calculated grating constant, a definite relationship between them is calibrated for the following experiments. The first-order diffraction efficiency is defined as the ratio of the first-order diffraction intensity to the incident laser intensity. The incident laser intensity is obtained from the fitting of the intensity distribution of Fig. 2(a), and the first-order diffraction intensity is obtained from Fig. 2(b). Thus we can get that the first-order diffraction efficiency of this grating is 25%.

From Eq. (1), we can see that the susceptibility of this system is sensitive to the atomic density. In thermal atom related experiments, atomic density is determined by the vapor temperature. In our experiment, we find a narrow temperature window for obtaining the clear diffraction pattern. The diffraction pattern can be obtained in a temperature range, but the clear pattern only appears in a small temperature window. The atomic density increases as the temperature increasing, which will give a larger refractive index contrast. However, an excessive atomic density causes the medium absorbs laser strongly, which will suppress this effect. The temperature of vapor cell in this experiment is controlled at 377.6 K, and the corresponding atomic density is about 1.0×10^{13} cm^{-3}.

The grating constant d is determined by the angle between the two coupling beams. Figure 3(a) shows the diffraction patterns with the angle φ varying from 0.10 to 0.26 degree, and Fig. 3(b) is the corresponding grating constant and the first-order diffraction efficiency. The error bars are the standard deviation of three experiment measurements. The grating constant decreases as the angle increases. The first-order diffraction efficiency is improved when the angle is gradually increasing from 0.10 to 0.20 degree, and it begins to decline when the angle reaches 0.20. The susceptibility of this system χ changes with the change of the angle, which can be seen from Eq. (1). The different susceptibility will result in different refractive index. With fine adjustment of the small angle between the two coupling lasers, we can obtain a clear diffraction pattern with a suitable refractive index. In order to observe clear discrete diffraction pattern, a small angle is needed to suppress the severe Doppler effect. When the angle is too small, the diffraction phenomenon is hard to be detected by the probe beam, which can be seen from Fig. 3(a1). But, too large angle induces a smaller grating constant, so that the diffraction patterns become dense and less distinguishable with low diffraction efficiency, which can be seen from Fig. 3(b). Thus, 0.20 degree is used in the following experiment.

When $\Delta_c = \Delta_p = 0$, $T_{phase}(x) = 0$ implies that no phase modulation takes place. At the transverse locations around the nodes of standing-wave, the probe beam is absorbed according to the usual Beer law where the coupling field is very weak. In contrast, at the transverse locations around the antinodes, the probe laser is absorbed much less due to the EIT effect. EIG is a kind of pure amplitude grating which tends to diffracting light into a central maximum, and limiting the light to stray into high order. While if the probe field is detuned off the resonance, a phase modulation will be introduced to its output profile rather than the nodes. In this case, the absorption and phase experience a rapid change in contrast to the amplitude modulation only. That is to say, the amplitude modulation tends to gather light to the center maximum while the phase modulation tends to disperse light into the higher order direction [7].

The formed hybrid (amplitude and phase) grating can enhance the efficiency of high order diffraction. We study the influence of the frequency detuning of probe field on the diffraction patterns in detail, which is shown in Fig. 4(a). The coupling laser frequency resonances on $5P_{3/2}(F = 2)$–$5D_{5/2}(F = 1)$ hyperfine transition, while the probe laser frequency is gradually tuned away from $5S_{1/2}(F = 2)$–$5P_{3/2}(F = 2)$ hyperfine transition, but it still operates in EIT window. The corresponding first-order diffraction efficiency with the variable two-photon frequency detuning is shown in Fig. 4(b). The red line is the theoretical fitting about the experimental results by Eq. (5). The errors are the standard deviation from three measurements. The theory and experiment are in qualitative agreement, a narrow frequency window exists for a good diffraction pattern. In Fig. 4(a1), the two-photon detuning is zero, a periodic amplitude modulation across the probe beam profile leading to a pure amplitude grating. The improvement of high order diffraction efficiency is limited in this case. The diffraction efficiency increases when the probe frequency is tuned away, and the optimized diffraction patterns appear at detuning of 20 MHz. As frequency detuning of probe field is removed away from this optimal point, the intensity of diffraction is decreased and the order of diffraction is reduced. When the two-photon detuning is too large, the diffraction efficiency reduces, and the medium becomes more transparent and the dispersion is weakened. The diffraction patterns of the probe beam disappear completely at two-photon detuning of 50 MHz.

The nonlinear enhancement of the EIT with the in-

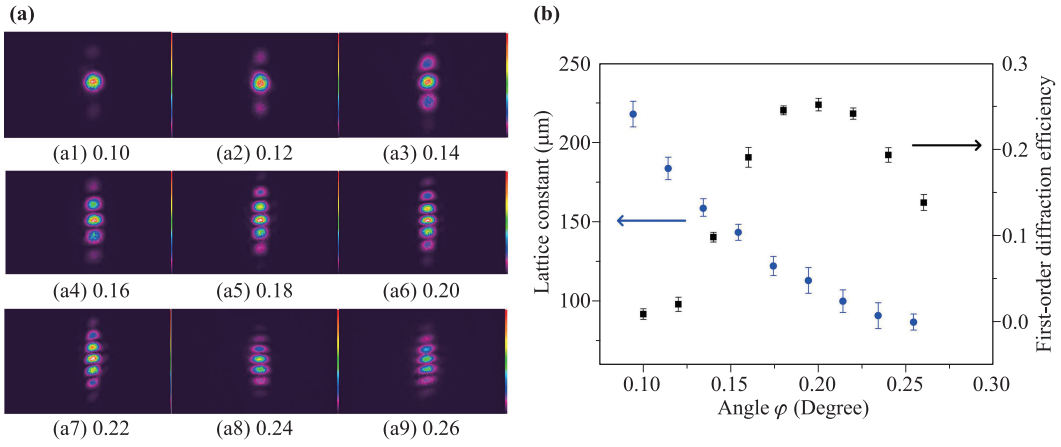

Fig. 3 **(a)** The diffraction patterns with different angles φ (in degree) of two coupling lasers. **(b)** The grating constant (circles) and the first-order diffraction efficiency (squares) as a function of the angle φ.

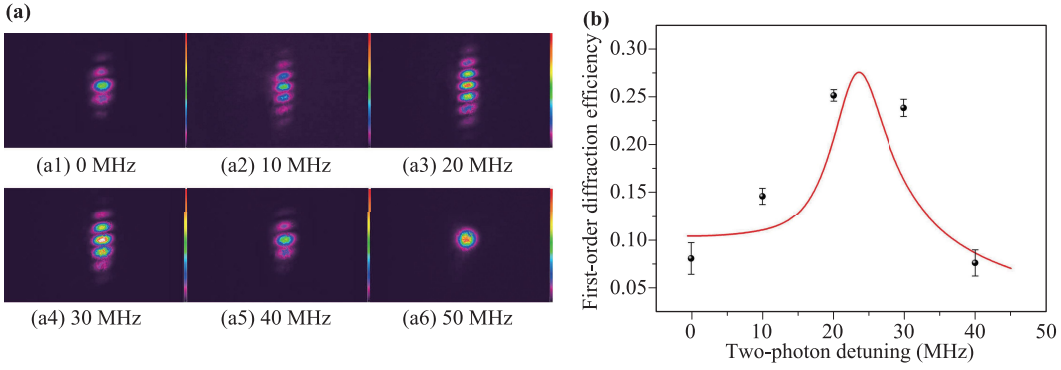

Fig. 4 **(a)** The output diffraction patterns with different two-photon detunings. **(b)** The corresponding first-order diffraction efficiency with different two-photon frequency detunings. The red line is the theoretical fitting and dots are experimental results.

creasing coupling laser intensity greatly contributes to the diffraction efficiency of high orders. Figure 5 shows the three-dimensional output diffraction patterns with different coupling laser powers. The diffraction efficiencies of each orders are visualized as a function of coupling laser powers. The diffraction efficiency of each order increases with the coupling laser power increases from 4 mW to 16 mW. Further increasing the laser power leads to a decrease in diffraction efficiency, which can be seen from the comparison between Figs. 5(e) and (f).

In order to study this effect in detail, we have measured more diffraction patterns with variable coupling laser powers. Figure 6 presents the corresponding first-order diffraction efficiency when the coupling laser power increasing from 4 mW to 30 mW. The red line is the theoretical fitting about the experimental results by Eq. (5), while the errors are the standard deviation from three measurements. When the standing-wave field acts on atoms, the diffraction of probe beam begins to appear at small power of 4 mW owing to EIG. The diffraction efficiencies of different orders gradually enhance with increasing the power of coupling laser. The coupling laser field reduce the near-resonance absorption of the probe field because of the EIT effect. This tendency is consistent with the theoretical prediction for a three-level system in Ref. [7]. When we increase the power of the coupling field, the EIT window will gradually open up the individual antinodes, which will allow more light available for diffraction into the first-order. However, for a strong coupling field, there will be a wide transparent regime within a single period of grating,

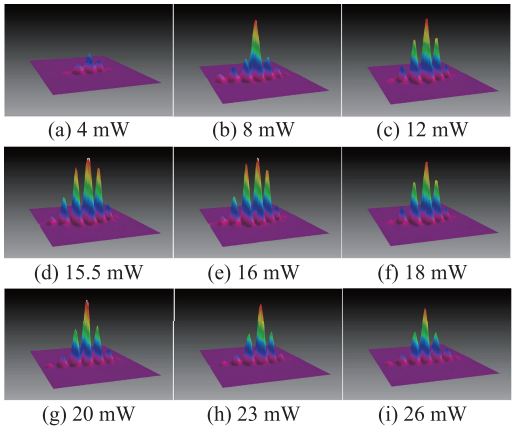

Fig. 5 The three-dimensional output diffraction patterns with different coupling laser powers.

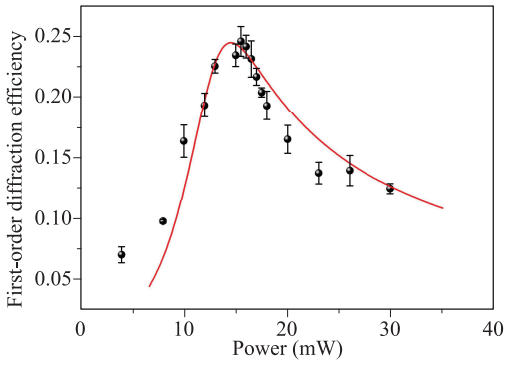

Fig. 6 The first-order diffraction efficiency of electromagnetically induced grating with different coupling laser powers. The red line is the theoretical simulation and dots are experimental results.

which possess a diffraction envelop highly concentrated along the forward direction, and reduce the chances of light to stray into the first-order. When the coupling laser power attains to 16 mW, the diffraction efficiency reaches a maximum value and a high contrast of the diffraction pattern is obtained. Then diffraction efficiency decreases with a further increasing of the coupling laser power. It shows that the present of a strong coupling field can suppressed the absorption of the probe field and render the grating transparent. Under the coupling laser power of 16 mW and other obtained optimized experimental parameters, the first, second and third order diffraction efficiency can reach to 25%, 9%, and 3%, respectively.

4 Conclusion

In summary, we have experimentally studied the electromagnetically induced grating diffraction controllability in a cascade-type coherent system of rubidium. The dependence of the grating characteristic parameters on angle of the two coupling lasers, two-photon detuning and coupling laser power are studied in detail. The optimal angle of 0.20 degree and two-photon detuning of 20 MHz are found to generate the high diffraction efficiency. The nonlinear dependence of the first-order diffraction efficiency on the coupling laser power is experimentally demonstrated for the first time, which is only theoretically predicted before. The maximum first-order diffraction efficiency is significantly enhanced to 25% when the coupling laser power is 16 mW. Further development of this atomic system will provide a potential platform for realizing new photonic devices and studying intriguing physical effects, such as electromagnetically induced Talbot effect [33, 34], non-Hermitian physics [35, 36], optical solitons [37].

Acknowledgements This work was supported by the National Key R&D Program of China (Grant No. 2017YFA0304203), the National Natural Science Foundation of China (Grant Nos. 61575116, 61875112, 61705122, 61728502, 91736209, and 11434007), Changjiang Scholars and Innovative Research Team in University of Ministry of Education of China (Grant No. IRT 17R70), the Program for Sanjin Scholars of Shanxi Province, Applied Basic Research Project of Shanxi Province (No. 201701D221004), Key Research and Development Program of Shanxi Province for International Cooperation (201803D421034), 111 project (Grant No. D18001) and the Fund for Shanxi "1331 Project" Key Subjects Construction.

References

1. S. E. Harris, Electromagnetically induced transparency, *Phys. Today* 50(7), 36 (1997)
2. M. Fleischhauer, A. Imamoglu, and J. P. Marangos, Electromagnetically induced transparency: Optics in coherent media, *Rev. Mod. Phys.* 77(2), 633 (2005)
3. L. V. Hau, S. E. Harris, Z. Dutton, and C. H. Behroozi, Light speed reduction to 17 metres per second in an ultracold atomic gas, *Nature* 397(6720), 594 (1999)
4. J. J. Longdell, E. Fraval, M. J. Sellars, and N. B. Manson, Stopped light with storage times greater than one second using electromagnetically induced transparency in a solid, *Phys. Rev. Lett.* 95(6), 063601 (2005)
5. Z. Xu, Y. Wu, L. Tian, L. Chen, Z. Zhang, Z. Yan, S. Li, H. Wang, C. Xie, and K. Peng, Long lifetime and high-fidelity quantum memory of photonic polarization qubit by lifting Zeeman degeneracy, *Phys. Rev. Lett.* 111(24), 240503 (2013)
6. Z. Wu, K. Chang, Y. Hu, Y. Zhang, Z. Jiang, and Y. Zhang, Modulation of four-wave mixing via photonic band gap, *Front. Phys.* 9(5), 665 (2014)
7. H. Ling, Y. Q. Li, and M. Xiao, Electromagnetically induced grating: Homogeneously broadened medium, *Phys. Rev. A* 57(2), 1338 (1998)
8. F. Bozorgzadeh, M. Sahrai, and H. Khoshsima, Controlling the electromagnetically induced grating via spontaneously generated coherence, *Eur. Phys. J. D* 70(9), 191 (2016)
9. A. W. Brown and M. Xiao, All-optical switching and routing based on an electromagnetically induced absorption grating, *Opt. Lett.* 30(7), 699 (2005)
10. A. André, M. Bajcsy, A. S. Zibrov, and M. D. Lukin, Nonlinear optics with stationary pulses of light, *Phys. Rev. Lett.* 94(6), 063902 (2005)
11. D. Moretti, D. Felinto, J. W. R. Tabosa, and A. Lezama, Dynamics of a stored Zeeman coherence grating in an external magnetic field, *J. Phys. At. Mol. Opt. Phys.* 43(11), 115502 (2010)
12. L. E. de Araujo, Electromagnetically induced phase grating, *Opt. Lett.* 35(7), 977 (2010)
13. M. Gao, Z. Wang, Z. Ullah, H. Chen, D. Zhang, Y. Zhang, and Y. Zhang, Modulated photonic band gaps generated by high-order wave mixing, *J. Opt. Soc. Am. B* 32(1), 179 (2015)

14. J. Tabosa, A. Lezama, and G. Cardoso, Transient Bragg diffraction by a transferred population grating: application for cold atoms velocimetry, *Opt. Commun.* 165(1–3), 59 (1999)
15. P. W. Zhai, X. M. Su, and J. Y. Gao, Optical bistability in electromagnetically induced grating, *Phys. Lett. A* 289(1–2), 27 (2001)
16. L. Zhao, W. Duan, and S. F. Yelin, All-optical beam control with high speed using image-induced blazed gratings in coherent media, *Phys. Rev. A* 82(1), 013809 (2010)
17. J. Wen, Y. Zhai, S. Du, and M. Xiao, Engineering biphoton wave packets with an electromagnetically induced grating, *Phys. Rev. A* 82(4), 043814 (2010)
18. M. Mitsunaga and N. Imoto, Observation of an electromagnetically induced grating in cold sodium atoms, *Phys. Rev. A* 59(6), 4773 (1999)
19. J. Sheng, J. Wang, M. A. Miri, D. N. Christodoulides, and M. Xiao, Observation of discrete diffraction patterns in an optically induced lattice, *Opt. Express* 23(15), 19777 (2015)
20. J. Yuan, Y. Li, S. Li, C. Li, L. Wang, L. Xiao, and S. Jia, Experimental study of discrete diffraction behavior in a coherent atomic system, *Laser Phys. Lett.* 14(12), 125206 (2017)
21. B. K. Dutta and P. K. Mahapatra, Electromagnetically induced grating in a three-level X-type system driven by a strong standing wave pump and weak probe fields, *J. Phys. At. Mol. Opt. Phys.* 39(5), 1145 (2006)
22. R. G. Wan, J. Kou, L. Jiang, Y. Jiang, and J. Y. Gao, Electromagnetically induced grating via enhanced nonlinear modulation by spontaneously generated coherence, *Phys. Rev. A* 83(3), 033824 (2011)
23. F. Zhou, Y. Qi, H. Sun, D. Chen, J. Yang, Y. Niu, and S. Gong, Electromagnetically induced grating in asymmetric quantum wells via Fano interference, *Opt. Express* 21(10), 12249 (2013)
24. Z. H. Xiao, L. Zheng, and H. Lin, Photoinduced diffraction grating in hybrid artificial molecule, *Opt. Express* 20(2), 1219 (2012)
25. S. Kuang, C. Jin, and C. Li, Gain-phase grating based on spatial modulation of active Raman gain in cold atoms, *Phys. Rev. A* 84(3), 033831 (2011)
26. L. Wang, F. Zhou, P. Hu, Y. Niu, and S. Gong, Two-dimensional electromagnetically induced cross-grating in a four-level tripod-type atomic system, *J. Phys. At. Mol. Opt. Phys.* 47(22), 225501 (2014)
27. A. Vafafard and M. Sahrai, Electromagnetically induced grating based on Zeeman coherence oscillations in cases beyond the multi-photon resonance condition, *J. Opt. Soc. Am. B* 35(9), 2118 (2018)
28. T. Naseri and R. Sadighi-Bonabi, Electromagnetically induced phase grating via population trapping condition in a microwave-driven four-level atomic system, *J. Opt. Soc. Am. B* 31(11), 2879 (2014)
29. T. Naseri and R. Sadighi-Bonabi, Efficient electromagetically induced phase grating via quantum interference in a four-level n-type atomic system, *J. Opt. Soc. Am. B* 31(10), 2430 (2014)
30. A. Vafafard and M. Mahmoudi, Switching from electromagnetically induced absorption grating to electromagnetically induced phase grating in a closed-loop atomic system, *Appl. Opt.* 54(36), 10613 (2015)
31. T. Naseri and R. Moradi, Realization of electromagnetically induced phase grating and Kerr nonlinearity in a graphene ensemble under Raman excitation, *Superlattices Microstruct.* 101, 592 (2017)
32. S. Wang, J. Yuan, L. Wang, L. Xiao, and S. Jia, Investigation on the monochromatic two-photon transition spectroscopy of rubidium by using intensity modulation method, *J. Phys. Soc. Jpn.* 87(8), 084301 (2018)
33. Z. Zhang, X. Liu, D. Zhang, J. Sheng, Y. Zhang, Y. Zhang, and M. Xiao, Observation of electromagnetically induced Talbot effect in an atomic system, *Phys. Rev. A* 97(1), 013603 (2018)
34. J. Yuan, C. Wu, Y. Li, L. Wang, Y. Zhang, L. Xiao, and S. Jia, Integer and fractional electromagnetically induced Talbot effects in a ladder-type coherent atomic system, *Opt. Express* 27(1), 92 (2019)
35. Z. Zhang, Y. Zhang, J. Sheng, L. Yang, M. A. Miri, D. N. Christodoulides, B. He, Y. Zhang, and M. Xiao, Observation of parity-time symmetry in optically induced atomic lattices, *Phys. Rev. Lett.* 117(12), 123601 (2016)
36. Z. Zhang, D. Ma, J. Sheng, Y. Zhang, Y. Zhang, and M. Xiao, Non-Hermitian optics in atomic systems, *J. Phys. At. Mol. Opt. Phys.* 51(7), 072001 (2018)
37. Y. Zhang, Z. Wang, Z. Nie, C. Li, H. Chen, K. Lu, and M. Xiao, Four-wave mixing dipole soliton in laser-induced atomic gratings, *Phys. Rev. Lett.* 106(9), 093904 (2011)